Optically induced coherent transport far above T_c in underdoped YBa$_2$Cu$_3$O$_{6+\delta}$

S. Kaiser,[1,*] C. R. Hunt,[1,4] D. Nicoletti,[1] W. Hu,[1] I. Gierz,[1] H. Y. Liu,[1] M. Le Tacon,[2] T. Loew,[2]
D. Haug,[2] B. Keimer,[2] and A. Cavalleri[1,3,†]

[1]*Max Planck Institute for the Structure and Dynamics of Matter, Hamburg, Germany*
[2]*Max Planck Institute for Solid State Research, Stuttgart, Germany*
[3]*Department of Physics, Oxford University, Clarendon Laboratory, Oxford, United Kingdom*
[4]*Department of Physics, University of Illinois at Urbana-Champaign, Urbana, Illinois, USA*

We report on a photoinduced transient state of YBa$_2$Cu$_2$O$_{6+\delta}$ in which transport perpendicular to the Cu-O planes becomes highly coherent. This effect is achieved by excitation with mid-infrared optical pulses, tuned to the resonant frequency of apical oxygen vibrations, which modulate both lattice and electronic properties. Below the superconducting transition temperature T_c, the equilibrium signatures of superconducting interlayer coupling are enhanced. Most strikingly, the optical excitation induces a new reflectivity edge at higher frequency than the equilibrium Josephson plasma resonance, with a concomitant enhancement of the low-frequency imaginary conductivity $\sigma_2(\omega)$. Above T_c, the incoherent equilibrium conductivity becomes highly coherent, with the appearance of a reflectivity edge and a positive $\sigma_2(\omega)$ that increases with decreasing frequency. These features are observed up to room temperature in YBa$_2$Cu$_2$O$_{6.45}$ and YBa$_2$Cu$_2$O$_{6.5}$. The data above T_c can be fitted by hypothesizing that the light establishes a transient superconducting state over only a fraction of the solid, with a lifetime of a few picoseconds. Non-superconducting transport could also explain these observations, although one would have to assume transient carrier mobilities near 10^4 cm^2/V sec at 100 K, with a density of charge carriers similar to the below-T_c superfluid density. Our results are indicative of highly unconventional nonequilibrium physics and open new prospects for optical control of complex solids.

PACS number(s): 74.25.N−, 74.25.Gz, 74.72.−h, 74.81.−g

Doped cuprates retain important properties of the superconducting state above the transition temperature T_c [1,2,3]. Charge transport in the normal state is highly incoherent, with low carrier mobilities [3]. Fluctuations of the order-parameter phase [4,5,6] and the emergence of competing orders [7,8] arise as coherence is lost when the temperature is raised above T_c. Magnetic fields affect this interplay, quenching superconducting coherence in favor of the competing phase [9,10]. In this work, we investigate the effect of optical excitation, with the goal of enhancing coherence and achieving the opposite effect of a magnetic field.

In the past, optical excitation has been applied almost exclusively at visible or near-infrared wavelengths, revealing information on the relaxation of hot incoherent quasiparticles back into the Cooper-pair condensate [11–13]. More recently, mode-selective optical deformation of the crystal lattice [14–16] has been used to affect the balance between competing phases on lower energy scales, transforming an insulating striped phase into a transient superconductor [17].

In the case of underdoped YBa$_2$Cu$_3$O$_{6+x}$, much work has been dedicated to understanding the properties of the normal state, unveiling a complex interplay of charge [8,18,19] and spin [20] order and possible above-T_c coherence [4,21]. These observations suggest that application of appropriate stimulation may reestablish superconducting order [22].

Three different underdoped compounds were studied in our experiments, YBa$_2$Cu$_3$O$_{6.45}$ (YBCO 6.45), YBa$_2$Cu$_3$O$_{6.5}$ (YBCO 6.5), and YBa$_2$Cu$_3$O$_{6.6}$ (YBCO 6.6), with corresponding hole doping levels of 7%, 9%, and 12%. Crystals of

typical dimensions $2 \times 2 \times 1$ mm^3 were grown in Y-stabilized zirconium crucibles [23]. The hole doping of the Cu-O planes was adjusted by controlling the oxygen content of the Cu-O chain layer δ by annealing in flowing O$_2$ and subsequent rapid quenching. The T_c values ($T_c = 35$ K for YBCO 6.45, $T_c = 50$ K for YBCO 6.5, and $T_c = 62$ K for YBCO 6.6) were determined by dc magnetization measurements in a SQUID, as discussed in the Supplemental Material [24].

For the purposes of the following discussion, it is important to note that equilibrium superconductors display a characteristic frequency-dependent conductivity $\sigma_1(\omega) + i\sigma_2(\omega)$, with a zero-frequency delta function in its real part $\sigma_1(\omega)$ and a positive imaginary part $\sigma_2(\omega)$ that diverges at low frequency as $1/\omega$. This frequency-dependent conductivity is clearly distinct from that of a Drude metal, for which charge carriers have a finite scattering time τ_s of only a few femtoseconds (10^{-15} sec). The real part of the conductivity is then constant for all frequencies smaller than the scattering rate $1/\tau_s$ ($\sim$ tens or hundreds of THz) and vanishes above it. The imaginary part $\sigma_2(\omega)$ is instead peaked at $1/\tau_s$, and tends to zero both at lower and higher frequencies.

For the case of layered cuprates, the difference between coherent and incoherent transport is underscored by further features of the optical properties. A zero crossing of the real part of the dielectric permittivity $\varepsilon_1(\omega)$ and a peak in the loss function $-\mathrm{Im}\{1/[\varepsilon_1(\omega) + i\varepsilon_2(\omega)]\}$ result in the appearance of a characteristic reflectivity edge at ω_J along the c axis, the so-called Josephson plasma resonance. This feature descents from self-sustained oscillations of the tunneling super-current between capacitively coupled plains. Above the superconducting transition temperature the reflectivity becomes featureless around ω_J, dominated by incoherent scattering at rates faster than the tunneling oscillations.

*Stefan.Kaiser@mpsd.mpg.de
†Andrea.Cavalleri@mpsd.mpg.de
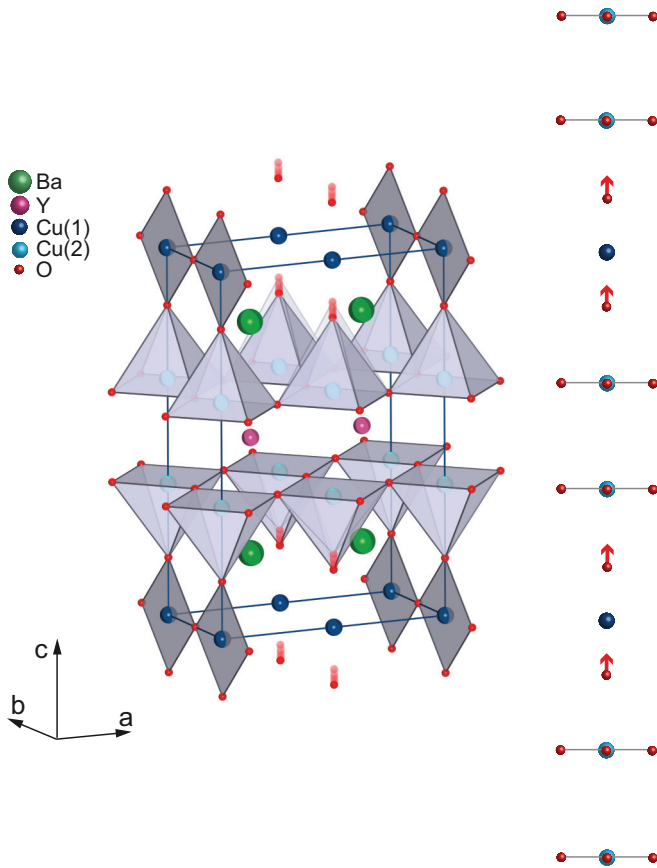
FIG. 1. (Color online) Structure of YBa$_2$Cu$_3$O$_{6.5}$ and lattice distortion for the 20-THz mode. Two conducting CuO$_2$ planes [Cu(2), and O in the *ab* plane] are separated by Y atoms (pink) and form a bilayer unit. Ba atoms (green) and the CuO$_4$ ribbons [Cu(1), and O in the *bc* plane) separate bilayer units [25]. The excitation of the infrared-active B$_{1u}$ mode at 20-THz frequency modulates only the displacement of the apical oxygen atoms along the *c* direction [26].

In the experiments reported here, changes in the equilibrium optical properties were induced by excitation with mid-infrared optical pulses of ~300 fs duration, polarized along the *c* direction and tuned to the 20 ± 3 THz frequency (~15 μm, 670 cm^{-1}, 83 meV, ±15%) of the infrared-active distortion of Fig. 1, which modulates the apical oxygen positions. The excitation pulses were generated by difference-frequency mixing in an optical parametric amplifier and focused onto the samples with a maximum fluence of 4 mJ/cm^2, corresponding to peak electric fields up to ~3 MV/cm. At this excitation level the vibrational mode was excited by several percent of the equilibrium bond distance.

The equilibrium and transient optical properties were probed in reflection between 0.5 and 2.5 THz [13,27]. Single-cycle THz pulses were generated by optical rectification of a near-infrared (800 nm wavelength) femtosecond pulse in a ZnTe crystal. The probe pulses were focused onto the YBCO crystals with polarization perpendicular to the superconducting planes (*c* axis), and were electro-optically sampled after reflection by a second near-infrared (800 nm wavelength) pulse in a second ZnTe crystal.
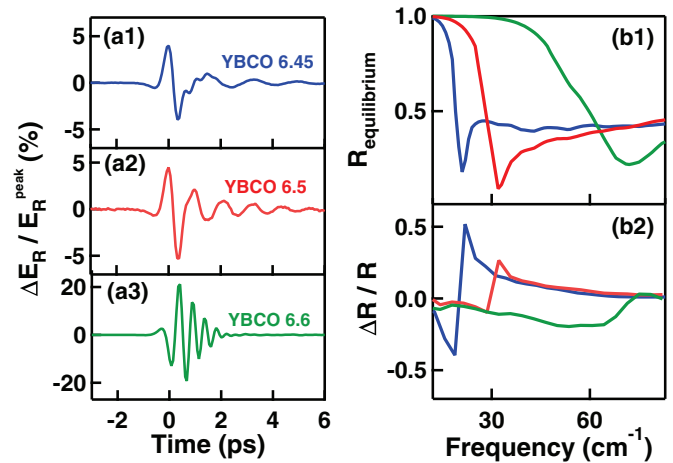
FIG. 2. (Color online) Below-T_c data. (a) Differential electric-field transient $\Delta E_R(t,\tau)/E_R(t^{\text{peak}})$ in YBCO 6.45 (blue), YBCO 6.5 (red), and YBCO 6.6 (green) excited with 20-THz pulses in the superconducting state at 20 K base temperature, measured with THz pulses polarized along the *c* axis (perpendicular to the superconducting planes). The response was measured at a time delay $\tau = +0.8$ ps after the 20-THz pump. (b1) Frequency-dependent reflectivities R_0 of YBCO 6.45, YBCO 6.5, and YBCO 6.6 measured at equilibrium along the *c* axis. Reflectivity edges of the Josephson plasma resonance are observed at $\omega_{J,6.45} \sim 20$ cm^{-1}, $\omega_{J,6.5} \sim 30$ cm^{-1}, and $\omega_{J,6.6} \sim 60$ cm^{-1}. (b2) Corresponding frequency-dependent differential changes in the reflectivities $\Delta R(\omega,0.8$ ps$)/R_0$ measured in (a1)–(a3) at positive time delays after the 20-THz pump. A shift of the Josephson plasma resonance is indicated.

Figure 2 summarizes the "raw" data obtained in the superconducting state (10 K base temperature). The equilibrium optical properties show reflectivity edges at $\omega_J \sim 20$ cm^{-1} for YBCO 6.45, $\omega_J \sim 30$ cm^{-1} for YBCO 6.5, and $\omega_J \sim 60$ cm^{-1} THz for YBCO 6.6 [Fig. 2(b)].

After excitation with the optical pump, the changes in the reflected electric field were recorded, as displayed in panels (a1)–(a3). Note that a clear oscillatory response is observed in these differential changes, dominated by a single frequency component that increases with increasing doping. From these curves, the differential electric field $\Delta E_R(t,\tau)$ and the stationary reflected electric field $E_R(t)$ were independently Fourier transformed to obtain the complex-valued, frequency-dependent $\Delta \tilde{E}_R(\omega)$ and $\tilde{E}_R(\omega)$. With knowledge of the equilibrium optical properties of the material the full complex optical response can be evaluated without using Kramers-Kronig relations.

The lower panel (b2) shows the corresponding reflectivity changes measured 0.8 ps after the photoexcitation [28], where the signal was maximum. For each doping level, we observed the strongest change around ω_J, with a reduction below the resonance and an enhancement above, indicating a blueshift of the plasma edge.

By analyzing the amplitude and phase of the transient reflectivity changes, taking into account the equilibrium optical properties and the mismatch between the penetration depths of mid-IR pump and the THz-probe beam (see Supplemental Material [24]), we determine the transient optical conductivity
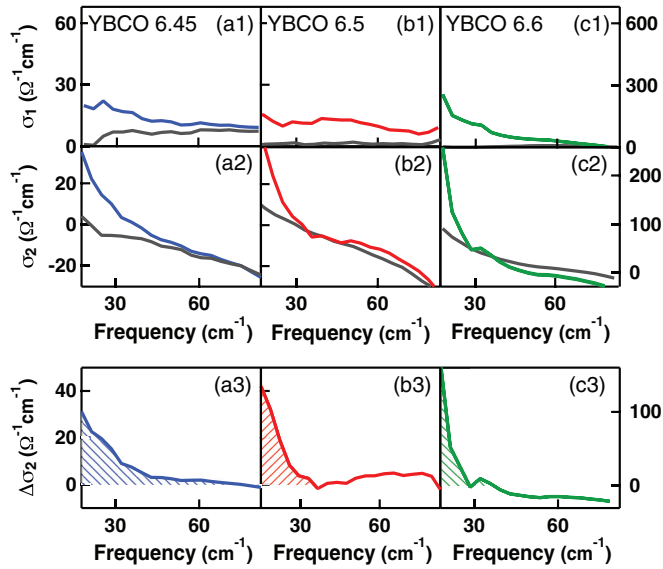
FIG. 3. (Color online) Below-T_c data. Optical properties of (a) YBCO 6.45, (b) YBCO 6.5, and (c) YBCO 6.6 in the superconducting state at 10 K base temperature. The gray lines describe the optical properties at equilibrium while the colored lines the response in the photostimulated state 0.8 ps after the excitation. The upper rows show σ_1, the real part, and σ_2, the imaginary part, of the complex optical response. The bottom row shows the photoinduced differential optical conductivity $\Delta\sigma_2$ between the optical properties in the photostimulated and the equilibrium state.

$\sigma_1(\omega) + i\sigma_2(\omega)$ in the photoexcited volume alone. Figure 3 displays the results of this analysis for YBCO 6.45, 6.5, and 6.6 in which the equilibrium optical properties are presented as gray lines, with the top panels indicating the real and imaginary part of the optical condutivities $\sigma_1(\omega)$ and $\sigma_2(\omega)$, respectively.

The response after photoexcitation with the mid-IR light pulses is presented with colored lines. The blue, red, and green lines show the optical properties in the photostimulated top layer at a pump-probe time delay of 0.8 ps after the photoexcitation in YBCO 6.45, 6.5, and 6.6. The real part of the optical conductivity is only slightly enhanced, likely due to moderate quasiparticle excitation. Crucially, the imaginary part shows a clear enhancement of the positive and diverging response. For a superconductor, the strength of this low-frequency divergence reflects an enhancement in the superfluid density, identified at equiliubrium as proportional to $\lim_{\omega\to 0}\omega\sigma_2$. This enhancement of the low-frequency σ_2 is opposite to the effect observed in photodoping experiments that break the superconducting condensate and in which the diverging σ_2 vanishes and a strong quasiparticle excitation sets in [13,27].

In Figs. 3(a3)–3(c3) we show also the transient photoinduced differential conductivity $\Delta\sigma_2$. These further emphasize the strong enhancement of the low-frequency σ_2 and therefore increase of the superfluid density. We find a stronger enhancement with a steeper divergence to lower frequencies when increasing the doping level.

Next we turn to base temperatures above the critical temperature T_c, where equilibrium transport is highly incoherent and the reflectivity featureless. Figure 4 summarizes the "raw" data measured in photoexcited YBCO 6.45 ($T_c = 35$ K).
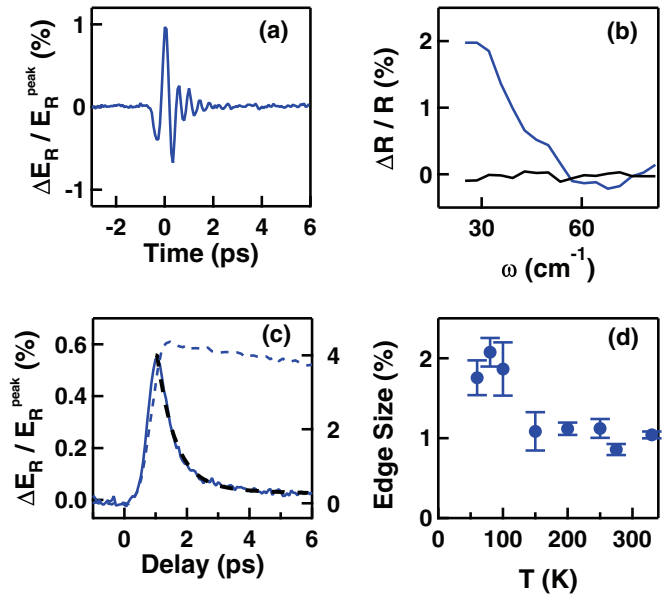
FIG. 4. (Color online) Above-T_c data. (a) Differential electric field transient $\Delta E_R(t,\tau)/E_R(t^{\text{peak}})$ in YBCO 6.45, excited with 20-THz pulses at 100 K base temperature. The response is measured with THz pulses polarized along the c axis (perpendicular to the superconducting planes) at a positive time delay ($\tau = +0.8$ ps) after the 20-THz pump. (b) Frequency-dependent reflectivity changes measured along the c axis. The black line describes the equilibrium response at negative pump-probe time delays and the blue curve the response 0.8 ps excitation. A photoinduced reflectivity edge is observed at $\omega_{J,6.45} \sim 43$ cm^{-1}. (c) Delay dependence of the peak THz signal $\Delta E_R(t^{\text{peak}},\tau)/E_R(t^{\text{peak}})$ as measured by scanning the pump-probe delay τ for YBCO 6.45. $\Delta E_R(t^{\text{peak}},\tau)$ is proportional to the frequency-integrated effect. For comparison the blue dashed line describes the response below T_c. (d) The size of the photoinduced reflectivity edge as function of base temperature.

Panel (a) displays the measured changes in the transient reflected THz field at 0.8 ps after the mid-IR excitation pulse. The corresponding frequency-resolved change in above-T_c reflectivity is reported in panel (b). A reflectivity edge of about 2% already in the raw data. The time-dependent response of the transient state is shown in panel (b) for the peak of the transient field changes. The lifetime of the light-induced state involves two decay time scales of ~0.5 ps and ~5–7 ps. We note that the narrow spectral width of the photoinduced edge of about ~20 cm^{-1} requires a lifetime of the state of more than 2 ps. We attribute the short time scale to the quasiparticle dynamics during the decay of the photoexcited state, which is discussed in more detail in our quantitative analysis. In contrast, the lifetime of the below-T_c response, shown as a dashed blue line, exhibits basically a single-exponential decay and lasts more than 10 ps. The size of this reflectivity edge is still about 1% when the temperature is increased up to 330 K as reported in the temperature dependence in panel (d).

As done for the below-T_c data, we analyze the amplitude and phase of the measured reflectivity transient taking into account the pump-probe penetration depth mismatch, and we determine the complex optical conductivity $\sigma_1(\omega) + i\sigma_2(\omega)$ of the photoexcited volume. Figure 5 displays the results of this
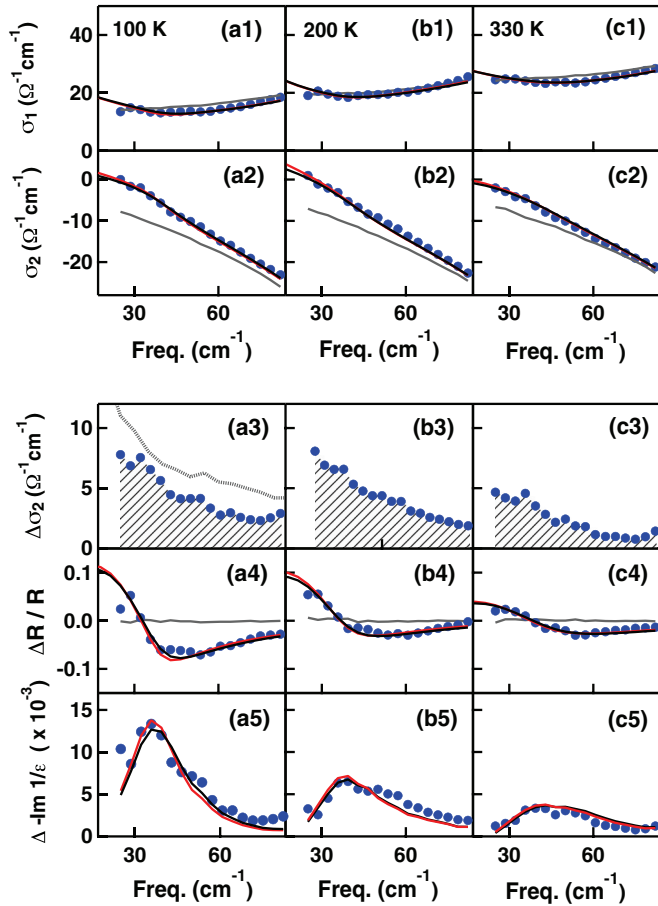
FIG. 5. (Color online) Optical properties YBCO 6.45 above T_c. 0.8 ps time delay after excitation at (a) 100 K, (b) 200 K, and (c) 330 K. Blue dots: Light-induced optical properties. Gray lines: Properties of the equilibrium state. Black lines: Effective medium fit for a transient conductor with $\tau_s = 7$ ps. Red lines: Effective medium fit for a perfect conductor with infinite lifetime. (a1)–(c1) Real part of the optical conductivity $\sigma_1(\omega)$. (a2)–(c2) Imaginary part of the optical conductivity $\sigma_2(\omega)$. (a3)–(c3) Differential changes in the imaginary conductivity $\Delta\sigma_2(\omega, 1\mathrm{ps}) = \sigma_2(\omega, 1\mathrm{ps}) - \sigma_2^0(\omega)$, where σ_2^0 is the equilibrium conductivity. Gray dotted curve: Change in imaginary conductivity $\Delta\sigma_2(\omega, \Delta T) = \sigma_2^0(\omega, 10\mathrm{K}) - \sigma_2^0(\omega, 60\mathrm{K})$ measured at equilibrium when cooling below T_c. (a4)–(c4) Light-induced changes in reflectivity. Gray line: Change in reflectivity measured at negative time delays (no signal). (a5)–(c5) Light-induced changes in the energy loss function $\Delta(-\mathrm{Im}1/\tilde{\varepsilon})$.

analysis for YBCO 6.45 at three temperatures (100 K, 200 K, 330 K). A virtually unchanged real part of the conductivity $\sigma_1(\omega)$ [panels (a1)–(c1)] is accompanied by an increase and a change of slope in the imaginary part $\sigma_2(\omega)$ [panels (a2)–(c2)], which becomes positive and increases for decreasing ω (blue points). Most strikingly, in panels (a3)–(c3) the corresponding change in imaginary conductivity $\sigma_2(\omega)$ [difference between the two curves in panels (a2)–(c2)] displays an approximate $1/\omega$ divergence over this frequency range.

From the optical properties extracted above, we also calculate the reflectivity changes that one would observe if the entire probed depth were excited [Figs. 5(a4)–5(c4)], yielding a rescaled edge with respect to that already reported
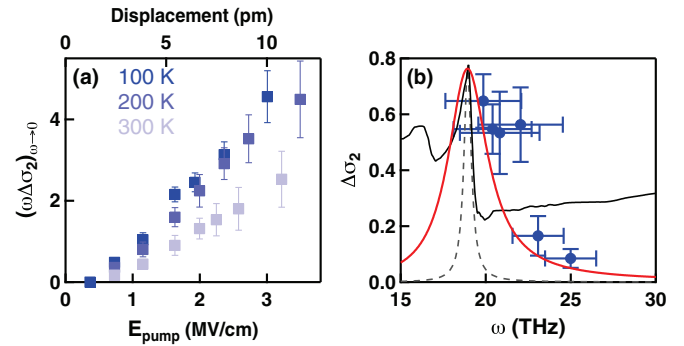
FIG. 6. (Color online) Fluence and wavelength dependence. (a) Size of the photoinduced enhancement $\omega\Delta\sigma_2$ for different pump fluences at 100 K, 200 K, and 300 K. The corresponding estimated displacement of the oxygen atoms (see Supplemental Material [24]) is shown in the top axis. (b) $\Delta\sigma_2$ at 1 THz plotted as a function of pump wavelength (blue dots) and measured at constant pump fluence. The horizontal bars indicate the pump spectral linewidth. The black line indicates equilibrium $\sigma_1(\omega)$. The resonant frequency of the apical oxygen mode is indicated in the dashed black curve, and in the red curve when convolved with the pump-pulse frequency bandwidth.

in Fig. 4(b). The corresponding changes in the energy loss function $\Delta(-\mathrm{Im}1/\varepsilon)$ are presented in Figs. 5(a5)–5(c5) peaking at the frequency of the photoinduced reflectivity edge. The fluence and wavelength dependence of the photoinduced effects are shown in Fig. 6. These increase linearly with the electric field of the mid-IR excitation pulses [Fig. 6(a)]. Secondly, the response is only observed in resonance with the IR-active apical oxygen mode at 15 μm [Fig. 6(b)].

Figures 7 and 8 show the corresponding temperature dependence of the optical response above T_c for YBCO 6.5 and YBCO 6.6. We find a transient response similar to that of YBCO 6.45, with an enhancement of the low-frequency $\sigma_2(\omega)$, the appearance of a plasma edge in the reflectivity, and a peak in the photoinduced loss function. However, when increasing doping an increasing response in the real part of the optical conductivity $\sigma_1(\omega)$ is observed, suggesting that some of the pump energy is exciting incoherent quasiparticles. With increasing doping level the photoinduced effect becomes stronger. The photoinduced plasma edge shifts to the blue, tracking the blueshift in the Josephson plasma edge observed in equilibrium below T_c. However, the temperature scale of the transient state does not track equilibrium superconductivity; instead the size of the effect drops more rapidly with temperature at higher dopings. In YBCO 6.6 the effect has entirely disappeared by 300 K, as shown in Fig. 8(c). The transient reflectivity is flat and $\Delta\sigma_2(\omega)$ is negative.

To quantitatively fit the temperature-dependent data, we first note that the reflectivity edge does not change in frequency with increasing temperature, in apparent contradiction with the decrease in $\Delta\sigma_2(\omega)$. This is interpreted as evidence for a state in which only a fraction of the material is transformed, embedded in a medium that remains incoherent. By assuming a high mobility state with constant local carrier density, but distributed in progressively sparser domains within the unperturbed normal state, these optical properties can be fitted very closely.
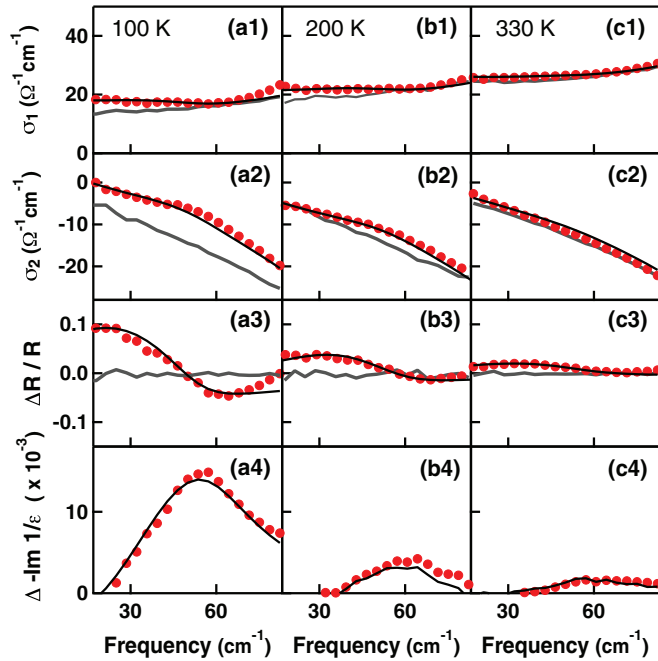
FIG. 7. (Color online) Optical properties YBCO 6.5 above T_c. 0.8 ps time delay after excitation at (a) 100 K, (b) 200 K, and (c) 330 K. Red dots: Light-induced optical properties. Gray lines: Properties of the equilibrium state. Black lines: Effective medium fit for a transient conductor with $\tau_s = 7$ ps. (a1)–(c1) Real part of the optical conductivity $\sigma_1(\omega)$. (a2)–(c2) Imaginary part of the optical conductivity $\sigma_2(\omega)$. (a3)–(c3) Light-induced changes in reflectivity. Gray line: Change in reflectivity measured at negative time delays (no signal). (a4)–(c4) Light-induced changes in the energy loss function $\Delta(-\text{Im}1/\tilde{\varepsilon})$.

FIG. 8. (Color online) Optical properties YBCO 6.6 above T_c. 0.8 ps time delay after excitation at (a) 100 K, (b) 150 K, and (c) 300 K. Green dots: Light-induced optical properties. Gray lines: Properties of the equilibrium state. Black lines: Effective medium fit for a transient conductor with $\tau_s = 7$ ps. (a1)–(c1) Real part of the optical conductivity $\sigma_1(\omega)$. (a2)–(c2) Imaginary part of the optical conductivity $\sigma_2(\omega)$. (a3)–(c3) Light-induced changes in reflectivity. Gray line: Change in reflectivity measured at negative time delays (no signal). (a4)–(c4) Light-induced changes in the energy loss function $\Delta(-\text{Im}1/\tilde{\varepsilon})$.

A quantitative fit to the data was obtained by applying the Bruggeman [29,30] effective dielectric function $\tilde{\varepsilon}_E(\omega)$ for an inhomogeneous medium: $f\frac{\tilde{\varepsilon}_{HM}(\omega)-\tilde{\varepsilon}_E(\omega)}{\tilde{\varepsilon}_{HM}(\omega)+2\tilde{\varepsilon}_E(\omega)} + (1-f)\frac{\tilde{\varepsilon}_{NS}(\omega)-\tilde{\varepsilon}_E(\omega)}{\tilde{\varepsilon}_{NS}(\omega)+2\tilde{\varepsilon}_E(\omega)} = 0$. We considered a mixture of a high-mobility conductor with dielectric function $\tilde{\varepsilon}_{HM}(\omega)$ of volume fraction f, which contains the photoinduced plasma edge, and of normal-state, unperturbed YBCO with the experimentally determined equilibrium $\tilde{\varepsilon}_{NS}(\omega)$ [31]. The experimental observations are fitted by letting only the plasma frequency ω_P and the transformed volume fraction f vary as free parameters [32], yielding curves that closely match the experimental observations (see black curves in Figs. 5, 7, and 8).

In Fig. 9, the key observations are summarized. We show an increase in $\sigma_2(\omega)$, and the appearance of a reflectivity edge and the corresponding loss function peak are shown for YBCO 6.45, YBCO 6.5, and YBCO 6.6 at 100 K for a direct comparison. We identify the increase of the inductive response in the differential optical conductivity $\Delta\sigma_2(\omega)$ and in the photoinduced plasma edge. The plasma frequency and the corresponding loss function peak increase with increasing doping level. Note once again how the photoinduced reflectivity edge and loss function peak are still observed at room temperature in YBCO 6.45 and YBCO 6.5, but they are no longer present in YBCO 6.6.

The results of the fits are summarized in Fig. 10. In panels (a1) and (a2), we show the optical conductivity of the normal state $\tilde{\varepsilon}_{NS}(\omega)$ (as extracted from literature data [31]) and of the transformed regions, $\tilde{\varepsilon}_{HM}(\omega)$. Most conservatively, these optical conductivities could be fitted by assuming that the transformed volume consists of a gas of noninteracting Drude electrons with conductivity $\tilde{\sigma}(\omega) = \omega_p^2/4\pi(1/\tau - i\omega)$ [33] with the experimentally determined plasma frequency $\omega_p^2 = (4\pi ne^2)/m_e$ and a scattering time $\tau = 7$ ps, corresponding to the lifetime of the photoinduced state, as extracted from the measurement in Fig. 4(b). With this model we can fit all temperatures and doping levels, and over the full range of measured fluences (see Supplemental Material [24]). Fits are shown as black lines in Figs. 5, 7, 8, and 9. From the simple Drude model we extract a dc mobility $\mu = e\tau/m_e \sim 12\,000$ cm^2/V s. We stress that such high mobility is highly unusual for c-axis transport in oxides, comparing favorably even with modulation-doped GaAs heterostructures in the same temperature range. Carrier mass renormalization would lower the effective mobility [2,3].

A transient superconducting state with lifetime $\tau_L \sim 7$ ps would exhibit the same ac optical properties as a Drude conductor with scattering time $\tau_S = \tau_L$. Since the minimum frequency measured here is greater than $1/\tau_L$, the transient state can be equally well described assuming the transformed volume is an equilibrium superconductor, i.e., $\tau_L \to \infty$ (red lines in same figures), but could not be fitted with scattering times below the lifetime of the state. At room temperature, this corresponds to effective scattering times of about 2 ps, which
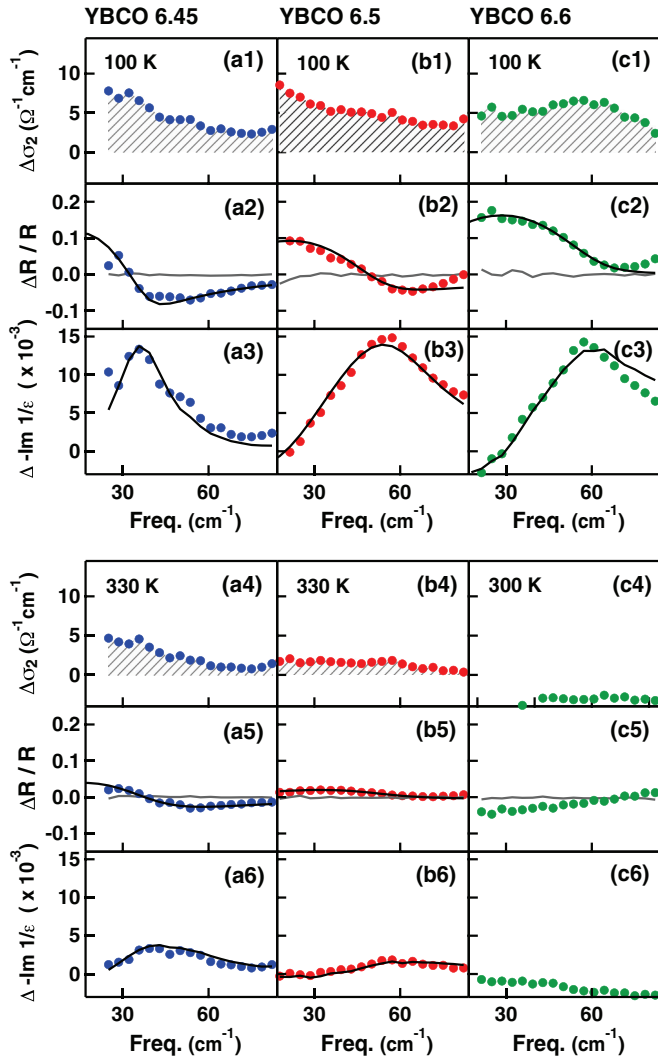
FIG. 9. (Color online) Doping-dependent transient optical properties of (a) YBCO 6.45, (b) YBCO 6.5, and (c) YBCO 6.6, 0.6 ps time delay after excitation (dots) at 100 K and high temperature. (a1)–(c1) Dots: Light-induced change in the optical conductivity $\sigma_2(\omega)$ at 100 K. (a2)–(c2) Dots: Light-induced changes in reflectivity at 100 K. Black line: Effective medium fit. Gray line: Change in reflectivity measured at negative time delays (no signal). (a3)–(c3) Dots: Light-induced changes in the imaginary conductivity $\Delta\sigma_2(\omega)$ at 330 K (YBCO 6.45 and YBCO 6.5) and 300 K (YBCO 6.6). (a5)–(c5) Dots: Light-induced changes in reflectivity at 330 K (YBCO 6.45 and YBCO 6.5) and 300 K (YBCO 6.6). Black line: Effective medium fit. Gray line: Change in reflectivity measured at negative time delays (no signal). (a6)–(c6) Dots: Light-induced changes in the energy loss function at 330 K (YBCO 6.45 and YBCO 6.5) and 300 K (YBCO 6.6). Black line: Effective medium fit.

would reduce the extracted mobility by a factor of about 3.5 compared to the above.

The value of the plasma frequency ω_p used to fit the data for each doping value is almost independent of the base temperature, whereas the volume fraction f extracted with the fit decreases with increasing temperature (see below). In Figs. 10(b1)–10(b3) we display the temperature dependence of f for the three different doping levels measured. A temperature

scale T' for the light-induced high-mobility phase is established by fitting the temperature-dependent volume fraction with an empirical mean-field law of the type $\propto \sqrt{1 - T/T'}$. The fitted T' values ($T'_{6.45} = 370 \pm 25$ K, $T'_{6.5} = 330 \pm 10$ K, and $T'_{6.6} = 160 \pm 20$ K) are visually reported in the phase diagram Fig. 11 where the blue shaded area indicates the region where we can photoinduce a coherent high-mobility state with scattering times always as long as, or even longer than, the lifetime of the transient state.

The interpretation of a high-mobility Drude conductor is in our view unlikely, as the density of photoexcited carriers should depend on the laser fluence and with it the position of the plasma edge. On the other hand, in our experiments only the fraction of optically transformed material is a function of laser field, but the position of the edge does not depend on the number of absorbed photons (see Supplemental Material [24]).

An alternative effect that could give rise to such high-mobility transport may be conduction by a noncommensurate sliding one-dimensional charge density wave [34], which could become depinned when the lattice is modulated and pin again a few picoseconds after excitation. Indeed, as charge density waves have been observed in this doping range, this possibility should be considered as a possible explanation.

However, many more observations support an interpretation for the above-T_c data based on transient superconducting coherence. First of all one can compare all the light-induced changes reported here to the observations made for the transient state induced below T_c.

As discussed in Fig. 3 a clear photoinduced enhancement of the superconducting state is seen below T_c, as underscored by a blueshift of the Josephson plasma edge and the strong increase in the divergence of the low-frequency $\sigma_2(\omega)$. Furthermore the photoinduced change $\Delta\sigma_2(\omega)$ in imaginary conductivity above T_c displayed in Figs. 5(a3)–5(c3) tracks very well the superconducting component of the equilibrium inductive conductivity below T_c, $\Delta\sigma_2(\omega) = \sigma_2(\omega, 10\text{ K}) - \sigma_2(\omega, 60\text{ K})$, which is indicated by a gray dashed curve in Fig. 5(a3). This similarity is further underscored by the observation that the position at which the plasma edge is being generated is very close to the equilibrium Josephson plasma resonance. Also, the frequency of the light-induced edge shifts to higher frequencies for increasing static doping, in analogy with the equilibrium Josephson plasma resonance [31] (see Fig. 2(b1) and Supplemental Material [24]).

To identify the physical mechanisms that may cause transient superconductivity, we first note how photoinduced redistribution of quasiparticles [35,36], which was shown in the past to enhance superconductivity at microwave [37–41] or optical [42,43] frequencies, is an unlikely explanation. The light-induced state can be created only when the pump wavelength is tuned to the phonon resonance (see Fig. 6), disappearing at higher frequency. This wavelength dependence is incompatible with charge excitations, which should persist at photon energies higher than the phonon frequency.

Rather, excitation of the lattice may be "melting" an ordered state that competes with superconductivity, as shown in the past for striped cuprates and for other complex materials. In underdoped YBCO, the recent discovery of a charge density wave (CDW) that competes with superconductivity [8] provides an appealing physical framework for this effect.
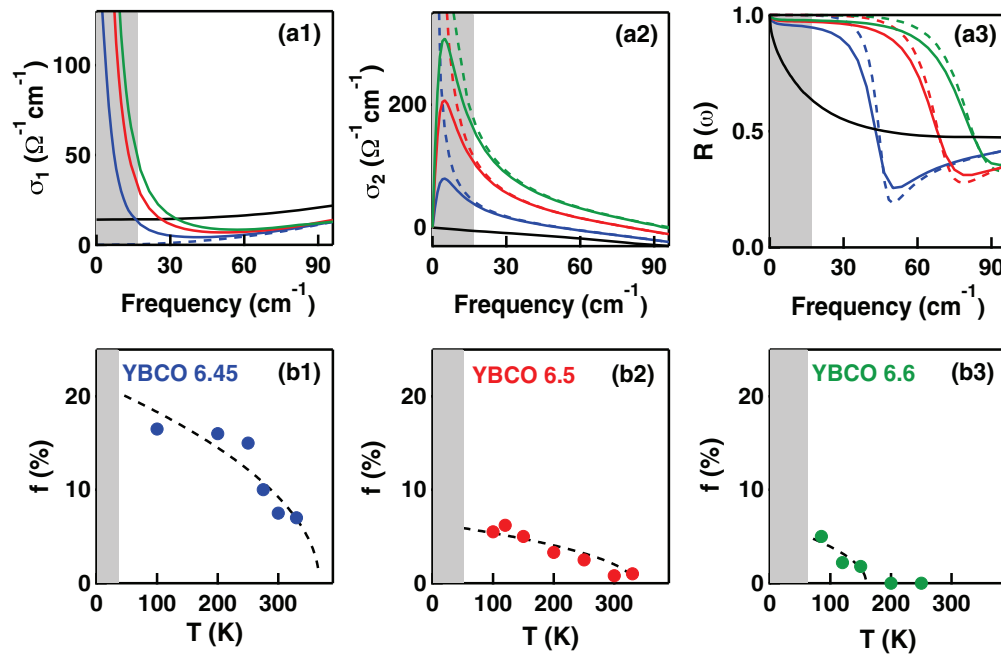
FIG. 10. (Color online) Results of the effective medium analysis. (a1)–(a3) Black curve: Optical properties of the unperturbed material. Blue curves: Extracted optical properties for the light-induced phase in YBCO 6.45 at 100 K [$\sigma_1(\omega)$ in panel (a1), $\sigma_2(\omega)$ in panel (a2), reflectivity in panel (a3)]. Red curves: Extracted optical properties for the light-induced phase in YBCO 6.5 at 100 K. Green curves: Extracted optical properties for the light-induced phase in YBCO 6.6 at 100 K. Solid lines assume a solid that exhibits perfect transport for the 7 ps lifetime of the state. Dashed curves represent the optical properties of a perfect conductor with infinitely long lifetime. Both assumptions provide a satisfactory fit in our spectral range. (b1)–(b3) Fitted filling fraction as a function of temperature. The dashed curves are fits obtained with an empirical mean-field dependence of the type $\propto \sqrt{1 - \frac{T}{T'}}$.

On the other hand, the anticorrelation of the light-induced superconducting volume fraction f [Fig. 10(b)] with the
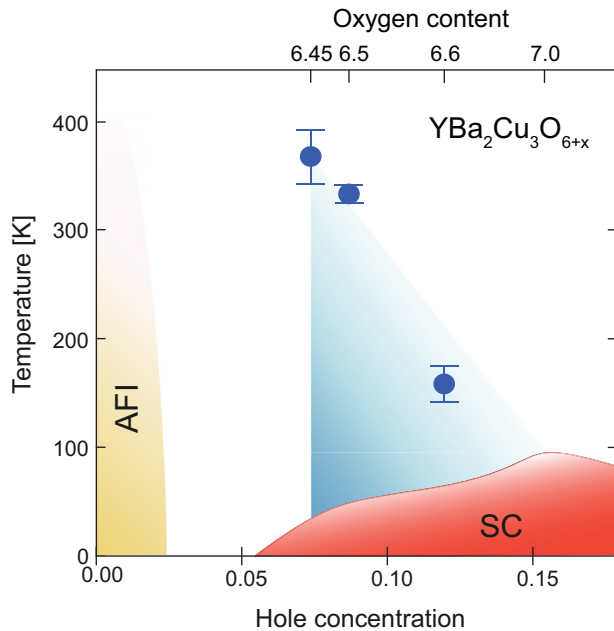
FIG. 11. (Color online) Schematic phase diagram of YBCO, where the equilibrium phases (superconducting and antiferromagnetic), as well as the nonequilibrium phase discussed in this paper, are displayed. The blue dots are the T' values extracted from the fits in Figs. 10(b1)–10(b3).

equilibrium CDW amplitude measured upon doping would argue against a scenario in which light illumination primarily modulates the balance between CDW and superconducting phases. It is interesting to note that f does correlate with the spectral weight of low-energy spin excitations, which is most pronounced in YBCO 6.45 and decreases strongly with both doping [44] and temperature dependence [45].

A second possibility is that the nonlinear coherent phonon excitation [46,47] may be transiently creating a displaced crystal structure with atomic positions more favorable to high-temperature superconductivity. Indeed, appropriate displacements of the apical oxygen away from the planes may promote coherence [48–52]. Finally, one should also consider the possibility of a coherent state induced by rapid modulation. As the 20 THz modulation used here occurs at frequencies high compared to plasma excitations between planes, one could envisage a dynamically stabilized stack of Josephson-coupled planes [53]. An instructive analogy can be drawn with other physical systems in which coherence is enhanced by rapid modulation, as observed in classical mechanics [54,55] or in nuclear magnetic resonance [56]. The lifetime of the state (see Fig. 2) is compatible with the dephasing time of the driven infrared-active vibration.

In summary, we have used vibrational excitation in the mid-infrared to induce a transient state in YBCO 6+δ with enhanced interlayer transport properties. Below T_c the data shows a clear enhancement of superconducting transport, including a blue shift of the equilibrium Josephson plasma resonance and an enhanced $\sigma_2(\omega)$. Above T_c, the incoherent

equilibrium state is changed to one with extraordinary high mobility with a density of charge carriers very close to those of the equilibrium superconductor. The optical data are fitted by assuming that the high-mobility state occupies a volume fraction that decreases with increasing temperature. Stronger pump fields, impossible in our apparatus, may make it possible to reach the percolation threshold for the high-mobility phase at which point one may observe a homogeneous phase, a qualitatively different response, and longer lifetimes.

Interpretations based on conduction by normal carriers with anomalously high mobility or by a transient superconducting state fit the data equally well. Our experiments may provoke new thinking on the nature of the normal state. We establish a temperature scale $T \gg T_c$ below which the system becomes a high-mobility conductor. There seems to be a very visual analogy between the onset temperatures of the nonequilibrium perfect conductor and the onset of the preexisting coherence found in optical measurements [4,21] or more likely even the pseudogap phase (see Fig. 11). Our fit suggests that high-mobility transport or transient superconductivity emerges from progressively sparser regions of the pseudogap, as if only a fraction of the materials were susceptible to being switched [57]. A challenge for future research will be to encapsulate our findings in a description of the physics of coherently modulated unconventional superconductors, as well as to optimize the effect to seek to increase its lifetime and the fraction of the transformed material.

[1] Z. A. Xu, N. P. Ong, Y. Wang, T. Kakeshita, and S. Uchida, Nature (London) **406**, 486 (2000).

[2] T. Timusk and B. Statt, Rep. Prog. Phys. **62**, 61 (1999).

[3] D. N. Basov and T. Timusk, Rev. Mod. Phys. **77**, 721 (2005).

[4] A. Dubroka, M. Rössle, K. W. Kim, V. K. Malik, D. Munzar, D. N. Basov, A. A. Schafgans, S. J. Moon, C. T. Lin, D. Haug, V. Hinkov, B. Keimer, Th. Wolf, J. G. Storey, J. L. Tallon, and C. Bernhard, Phys. Rev. Lett. **106**, 047006 (2011).

[5] V. J. Emery and S. A. Kivelson, Nature (London) **374**, 434 (1995).

[6] J. Corson, R. Mallozzi, J. Orenstein, J. N. Eckstein, and I. Bozovic, Nature (London) **398**, 221 (1999).

[7] J. M. Tranquada, B. J. Sternlieb, J. D. Axe, Y. Nakamura, and S. Uchida, Nature (London) **375**, 561 (1995).

[8] G. Ghiringhelli, M. Le Tacon, M. Minola, S. Blanco-Canosa, C. Mazzoli, N. B. Brookes, G. M. De Luca, A. Frano, D. G. Hawthorn, F. He, T. Loew, M. Moretti Sala, D. C. Peets, M. Salluzzo, E. Schierle, R. Sutarto, G. A. Sawatzky, E. Weschke, B. Keimer, and L. Braicovich, Science **337**, 821 (2012).

[9] B. Lake, H. M. Rønnow, N. B. Christensen, G. Aeppli, K. Lefmann, D. F. McMorrow, P. Vorderwisch, P. Smeibidl, N. Mangkorntong, T. Sasagawa, M. Nohara, H. Takagi, and T. E. Mason, Nature (London) **415**, 299 (2002).

[10] E. Hoffman, E. W. Hudson, K. M. Lang, V. Madhavan, H. Eisaki, S. Uchida, and J. C. Davis, Science **295**, 466 (2002).

[11] J. Demsar, B. Podobnik, V. V. Kabanov, Th. Wolf, and D. Mihailovic, Phys. Rev. Lett. **82**, 4918 (1999).

[12] R. A. Kaindl, M. Woerner, T. Elsaesser1, D. C. Smith, J. F. Ryan, G. A. Farnan, M. P. McCurry, and D. G. Walmsley, Science **287**, 470 (2000).

[13] R. D. Averitt, G. Rodriguez, A. I. Lobad, J. L. W. Siders, S. A. Trugman, and A. J. Taylor, Phys. Rev. B **63**, 140502(R) (2001).

[14] M. Rini, R. Tobey, N. Dean, J. Itatani, Y. Tomioka, Y. Tokura, R. W. Schoenlein, and A. Cavalleri, Nature (London) **449**, 72 (2007).

[15] A. D. Caviglia, R. Scherwitzl, P. Popovich, W. Hu, H. Bromberger, R. Singla, M. Mitrano, M. C. Hoffmann, S. Kaiser, P. Zubko, S. Gariglio, J.-M. Triscone, M. Först, and A. Cavalleri, Phys. Rev. Lett. **108**, 136801 (2012).

[16] M. Först, R. I. Tobey, H. Bromberger, S. B. Wilkins, V. Khanna, A. D. Caviglia, Y.-D. Chuang, W. S. Lee, W. F. Schlotter, J. J. Turner, M. P. Minitti, O. Krupin, Z. J. Xu, J. S. Wen, G. D. Gu, S. S. Dhesi, A. Cavalleri, and J. P. Hill, Phys. Rev. Lett. **112**, 157002 (2014).

[17] D. Fausti, R. I. Tobey, N. Dean, S. Kaiser, A. Dienst, M. C. Hoffmann, S. Pyon, T. Takayama, H. Takagi, and A. Cavalleri, Science **331**, 189 (2011).

[18] T. Wu, H. Mayaffre, S. Krämer, M. Horvatić, C. Berthier, W. N. Hardy, R. Liang, D. A. Bonn, and M.-H. Julien, Nature (London) **477**, 191 (2011).

[19] J. Chang, E. Blackburn, A. T. Holmes, N. B. Christensen, J. Larsen, J. Mesot, R. Liang, D. A. Bonn, W. N. Hardy, A. Watenphul, M. v. Zimmermann, E. M. Forgan, and S. M. Hayden, Nat. Phys. **8**, 871 (2012).

[20] S. Blanco-Canosa, A. Frano, T. Loew, Y. Lu, J. Porras, G. Ghiringhelli, M. Minola, C. Mazzoli, L. Braicovich, E. Schierle, E. Weschke, M. Le Tacon, and B. Keimer, Phys. Rev. Lett. **110**, 187001 (2013).

[21] E. Uykur, K. Tanaka, T. Masui, S. Miyasaka, and S. Tajima, Phys. Rev. Lett. **112**, 127003 (2014).

[22] W. Hu, S. Kaiser, D. Nicoletti, C. R. Hunt, I. Gierz, M. C. Hoffmann, M. Le Tacon, T. Loew, B. Keimer, and A. Cavalleri, Nat. Mater. (2014).

[23] S. I. Schlachter, U. Tutsch, W. H. Fietz, K.-P. Weiss, H. Leibrock, K. Grube, Th. Wolf, B. Obst, P. Schweiss, and H. Wühl, Int. J. Mod. Phys. B **14**, 3673 (2000).

[24] See Supplemental Material at http://link.aps.org/supplemental/10.1103/PhysRevB.89.184516 for details on the sample characterization, the derivation of the complex conductivity, the pump fluence dependence and the estimation of the peak lattice distortion.

[25] G. Calestani and C. Rizzoli, Nature (London) **328**, 606 (1987).

[26] G. Burns, F. H. Dacol, P. P. Freitas, W. König, and T. S. Plaskett, Phys. Rev. B **37**, 5171 (1988).

[27] A. Pashkin, M. Porer, M. Beyer, K. W. Kim, A. Dubroka, C. Bernhard, X. Yao, Y. Dagan, R. Hackl, A. Erb, J. Demsar, R. Huber, and A. Leitenstorfer, Phys. Rev. Lett. **105**, 067001 (2010).

[28] The time-dependent profile of the pump-induced changes is shown as the frequency-averaged response, which is the blue dashed line in Fig. 4(c).

[29] D. J. Hilton, R. P. Prasankumar, S. Fourmaux, A. Cavalleri, D. Brassard, M. A. El Khakani, J. C. Kieffer, A. J. Taylor, and R. D. Averitt, Phys. Rev. Lett. **99**, 226401 (2007).

[30] M. M. Qazilbash, M. Brehm, Byung-Gyu Chae, P.-C. Ho, G. O. Andreev, Bong-Jun Kim, Sun Jin Yun, A. V. Balatsky, M. B. Maple, F. Keilmann, Hyun-Tak Kim, and D. N. Basov, Science **318**, 1750 (2007).

[31] C. C. Homes, T. Timusk, D. A. Bonn, R. Liang, and W. N. Hardy, Physica C **254**, 265 (1995).

[32] The photoexcited volume $\tilde{\varepsilon}_{HM}(\omega)$ is constructed assuming a plasma resonance fitted to the transient data with a single fit parameter, ω_J. The background includes a single ~ 150 cm^{-1} phonon contribution fitted from the equilibrium superconducting properties which remains fixed in all fits. The remaining volume $\tilde{\varepsilon}_{NS}(\omega)$ is taken from the unperturbed optical properties. For YBCO 6.5 and 6.6, an additional incoherent component was added to $\tilde{\varepsilon}_{NS}(\omega)$ to account for the quasiparticle contribution to the transient state; this can be seen most clearly in YBCO 6.6 as a flat increase in the ohmic conductivity [Fig. 8(a1)]. This contribution is negligible in YBCO 6.45 up to 100 K, but becomes finite at higher temperatures and, especially, as one approaches optimal doping. This quasiparticle component evolves following the short decay time scale and can be modeled in our bandwidth range as a single parameter: a frequency-independent contribution to $\sigma_1(\omega)$ that affects only the nontransformed volume $1 - f$.

[33] M. Dressel and G. Grüner, *Electrodynamics of Solids* (Cambridge University Press, 2002).

[34] G. Gruener, *Density Waves in Solids* (Addison-Wesley Publishing Company, 1994).

[35] G. M. Eliashberg, JETP Lett. **11**, 114 (1970); B. I. Ivlev and G. M. Eliashberg, *ibid.* **13**, 464 (1971).

[36] C. S. Owen and D. J. Scalapino, Phys. Rev. Lett. **28**, 1559 (1972).

[37] P. W. Anderson and A. H. Dayem, Phys. Rev. Lett. **13**, 195 (1964).

[38] A. F. G. Wyatt, V. M. Dmitriev, W. S. Moore, and F. W. Sheard, Phys. Rev. Lett. **16**, 1166 (1966).

[39] A. H. Dayem and J. J. Wiegand, Phys. Rev. **155**, 419 (1967).

[40] R. Escudero and H. J. T. Smith, Phys. Rev. B **31**, 2725 (1985).

[41] S. I. Vedeneev, D. K. Maude, and J. M. Byrne, Phys. Rev. B **78**, 052509 (2008).

[42] G. Yu, C. H. Lee, A. J. Heeger, N. Herron, and E. M. McCarron, Phys. Rev. Lett. **67**, 2581 (1991).

[43] G. Nieva, E. Osquiguil, J. Guimpel, M. Maenhoudt, B. Wuyts, Y. Bruynseraede, M. B. Maple, and Ivan K. Schuller, Appl. Phys. Lett. **60**, 2159 (1992).

[44] D. Haug, V. Hinkov, Y. Sidis, P. Bourges, N. B. Christensen, A. Ivanov, T. Keller, C .T. Lin, and B. Keimer, New J. Phys. **12**, 105006 (2010).

[45] V. Hinkov, P. Bourges, S. Pailhès, Y. Sidis, A. Ivanov, C. D. Frost, T. G. Perring, C. T. Lin, D. P. Chen, and B. Keimer, Nat. Phys. **3**, 780 (2007).

[46] M. Först, C. Manzoni, S. Kaiser, Y. Tomioka, Y. Tokura, R. Merlin, and A. Cavalleri, Nat. Phys. **7**, 854 (2011).

[47] M. Först, R. Mankowsky, H. Bromberger, D. M. Fritz, H. Lemke, D. Zhu, M. Chollet, Y. Tomioka, Y. Tokura, R. Merlin, J. P. Hill, S. L. Johnson, and A. Cavalleri, Solid State Commun. **169**, 24 (2013).

[48] E. Pavarini, I. Dasgupta, T. Saha-Dasgupta, O. Jepsen, and O. K. Andersen, Phys. Rev. Lett. **87**, 047003 (2001).

[49] C. Weber, K. Haule, and G. Kotliar, Phys. Rev. B **82**, 125107 (2010).

[50] J. A. Slezak, J. Lee, M. Wang, K. McElroy, K. Fujita, B. M. Andersen, P. J. Hirschfeld, H. Eisaki, S. Uchida, and J. C. Davis, Proc. Natl. Acad. Sci. USA **105**, 3203 (2008).

[51] M. Mori, G. Khaliullin, T. Tohyama, and S. Maekawa, Phys. Rev. Lett. **101**, 247003 (2008).

[52] H. Sakakibara, H. Usui, K. Kuroki, R. Arita, and H. Aoki, Phys. Rev. Lett. **105**, 057003 (2010).

[53] G. Baskaran, arXiv:1211.4567.

[54] P. L. Kapitza, Zh. Eksp. Teor. Fiz. **21**, 588 (1951).

[55] L. D. Landau and E. M. Lifschitz, *Mechanics* (Pergamon, Oxford, 1976).

[56] A. W. Overhauser, Phys. Rev. **92**, 411 (1953).

[57] He Rui-Hua, M. Hashimoto, and H. Karapetyan, Science **331**, 1579 (2011).